

The late magmatic to subsolidus T - fO_2 evolution of the Lower Triassic A-type rhyolites (Silicic Superunit, Western Carpathians, Slovakia): Fe–Ti oxythermometry and petrological implications

Martin Ondrejka¹, Igor Broska² & Pavel Uher¹

¹Department of Mineralogy and Petrology, Faculty of Natural Sciences, Comenius University Bratislava, Mlynská dolina, Ilkovičova 6, 842 15 Bratislava, Slovakia; mondrejka@fns.uniba.sk

²Geological Institute, Slovak Academy of Sciences, Dúbravská cesta 9, 840 05 Bratislava, Slovakia

AGEOS Neskoro magmatický až subsolidový T - fO_2 vývoj spodnotriasových rhyolitov A- typu (silicikum, Západné Karpaty, Slovensko): oxytermometria Fe–Ti oxidov a petrologické implikácie

Abstract: Iron-titanium oxides represent significant mineral phase (≤ 1.5 vol. %) in the A-type rhyolites from the Silicic Superunit, Western Carpathians, central Slovakia. They are composed of magnetite, ilmenite, and rutile showing typical lamellae “trellis - sandwich” type texture as a result of oxy-exsolution of former Ti-rich magnetite. A composite type and complete decomposition of primary Ti-rich magnetite to a very fine lamellae aggregate of hematite/rutile or to the progressive C4 stage of Fe-rich rutile/hematite occurs in lesser extent. The compositional data show significant miscibility along the ilmenite–hematite join. The ulvöspinel component in magnetite reaches up to 18 mol. %, while the rutile is more uniform and close to end-member composition. However, in some cases rutile is enriched in Fe getting up to 5 wt. % FeO_{total} mainly with coexisting ilmenite–hematite. Fe–Ti oxide geothermometry yields a relatively smooth evolutionary T -trend ranging from late-magmatic to subsolidus/solidus stages with equilibrium temperatures from ~ 750 to ~ 400 °C and fO_2 values approaching the NiNiO buffer from $-0.76 \Delta \log fO_2$ (~ 626 °C) to $1.53 \Delta \log fO_2$ (~ 655 °C). The presence of Ti-rich magnetite, Ti-poor magnetite, ilmenite to hematite, and discrete rutile in rhyolitic magma point to a long termed process from orthomagmatic to a low-temperature subsolidus/solidus stage showing a gradual decrease of oxygen fugacity. The Fe–Ti oxide investigation indicates a relatively short-term storage of the Permian A-type silicic melt at shallow depths prior to eruption.

Key words: Western Carpathians, A-type rhyolite, oxygen fugacity, oxide thermometry, Fe–Ti oxides, magnetite, ilmenite

1. INTRODUCTION

Magnetite is the most common ferromagnetic iron-titanium (Fe–Ti) oxide of the felsic rocks. It has cubic inverse spinel structure and Fe cations occupying the tetrahedral and octahedral sites. Tetrahedral sites contain only Fe^{3+} , whereas octahedral sites contain both iron valences but with a dominance of Fe^{2+} . In the octahedral sites, the electrons can hop between Fe^{2+} and Fe^{3+} ions at room temperature, rendering magnetite an important half-metallic material. Magnetite octahedral sites can easily incorporate Ti, forming Ti-rich magnetite (“titanomagnetite”) or compositional transition between magnetite (Fe_3O_4) and ulvöspinel (Fe_2TiO_4) which is a common early orthomagmatic mineral phase in some silicic magmas. Besides magnetite and ulvöspinel, granitoid rocks also contain solid Fe–Ti solutions between ilmenite and hematite, known as titanohematites (e.g., Waychunas, 1991).

Pre-eruptive magmatic conditions (temperature, oxygen fugacity, and magma chemistry) can be effectively estimated from Fe–Ti oxide chemistry in silicic volcanic rocks (e.g., Carmichael,

1967; Ewart et al., 1975; Powell & Powell, 1977; Spencer & Lindsley, 1981; Andersen & Lindsley, 1985; Frost, 1991a; Ghiorsso & Sack, 1991; Shane, 1998; Zhu et al., 2002; Saito et al., 2004; Hammer, 2006; Ryabchikov & Kogarko, 2006; Shane et al., 2007; Ghiorsso & Evans, 2008). The Fe–Ti petrology applied in volcanic rocks provides information on character of the melt in the storage chamber prior to eruption. Other possibility how to estimate temperature during evolution of volcanic rocks include also saturation thermometers based on REE, Zr, and P solubility in zircon and monazite (e.g., Watson & Harrison, 1983; Montel, 1993). In the Western Carpathians, the Fe–Ti petrology has been applied in the Cenozoic granites (Šulgan, 1986), Pliocene basalts (Hurai et al., 1998), on pincinite rocks derived from deep-crustal, high-temperature anatexites (Huraiová et al., 2005) and in I-type granitoids (Broska et al., 2007; Broska & Petřík, 2011).

The aim of this study is to contribute to the evolution of Lower Triassic A-type rhyolites from the Silicic Superunit in the Western Carpathians by investigation of Fe–Ti oxide minerals, including the T - fO_2 estimation. The composition of abundant Fe–Ti oxides

coupled with the application of geothermometry and oxygen barometry shed new light upon pre-eruptive magmatic conditions in the storage chamber of Permian rhyolites. The late-magmatic to subsolidus alteration of the rhyolites were also inspected.

2. GEOLOGICAL SETTINGS

The A-type rhyolites form lava flows or ignimbrite layers in the Lower Triassic siliciclastic and carbonate sequences of the Muráň and Drienok nappes (Silicic Superunit in the Inner Western Carpathians) (Uher et al., 2002). The Silicic Superunit represents the tectonically uppermost Alpine nappe structures in the Western Carpathians and overlies the Veporic, Hronic, Gemeric, Meliatic, and Turnaica superunits. The Upper Permian to Upper Jurassic sedimentary sequences which are facially analogous to the Schneeberg and Mürzalpe nappes of the Juvavic Unit of the Northern Calcareous Alps is part of rock succession (Mello et al., 1997). The lower part of the Silicic Superunit belonging to the Werfen Formation is a sequence of continental to shallow marine shales to sandstones sediments (up to 500 m in thickness) containing also limestones and siliciclastic admixture from the Early Triassic age. The studied rhyolites form small bodies in the Lower Triassic sandstones and the shales of the Bódvaszilas beds (Vojtko, 2000).

The A-type rhyolitic rocks show common features of acid volcanics. The texture is porphyric with grano-lepidoblastic and in some parts a microfelsic groundmass. Fluidal texture also occurs in some places. Phenocrysts, 2–4 mm in size, are represented by corroded bipyramidal β -quartz and euhedral alkali feldspars, but these are commonly replaced by chessboard albite or fine-grained white mica aggregates (Uher et al., 2002).

The groundmass consists of a very fine-grained aggregate of quartz, feldspar, white mica, hematite pigment, and occasionally biotite, chlorite and accessory zircon, monazite-(Ce), xenotime-(Y), rutile, ilmenite, magnetite, hematite, and barite (Uher et al., 2002). Moreover, the rhyolite body at Tisovec-Rejkovo contains a unique REE–Y–(Th)–P–As–(Si)–(Nb)–(S) accessory assemblage of REE arsenate – phosphate – silicates solid solutions, REE carbonates and rarely cerianite-(Ce) – Ondrejka et al. (2007).

Geochronological study of Telgárt-Gregová rhyolite, based on EMP monazite dating suggests Middle/Upper Permian age of parental rhyolitic volcanism in the range of 263 ± 3.5 Ma (Demko & Hraško, 2013) which is coincident with previous data obtained for Poniky-Drienok (261 ± 15 Ma) and Veľká-Stožka (258 ± 12 Ma) rhyolitic bodies (Ondrejka, 2004).

Volcanic rocks of the Silicic Superunit are known in several places (cf. Uher et al., 2002; Ondrejka, 2004; Ondrejka et al., 2007; Demko & Hraško, 2013) but this paper is dealing with occurrences only from the Veľká Stožka-Dudlavka (SD), Telgárt-Gregová (TEL), Tisovec-Rejkovo (TIS) and Poniky-Drienok (PO) localities (Fig. 1).

3. METHODS AND CALCULATIONS

Fe–Ti oxides were studied in polished thin sections of the rhyolites. Electron microprobe analyses and back scattered

electron imaging (BSE) were obtained at the Slovak Geological Survey in Bratislava (ŠGÚDŠ), using the Cameca SX100, and at Salzburg University using the JEOL – 8600 microprobes operated in wavelength-dispersion mode. The analytical conditions were as follows: accelerating voltage 15 kV, beam current 20 nA, and a beam diameter from 0.7 to 4 μm . The following standards and spectral lines were utilized: TiO_2 (Ti K α), Al_2O_3 (Al K α), chromite (Cr K α), hematite (Fe K α), rhodonite (Mn K α), MgO (Mg K α), metallic nickel (Ni K α). The electron-microprobe data were reduced by the PAP-procedure. Special care was exercised to ensure that the analyses of the Fe–Ti phases were not mixtures. However in some cases it cannot be guaranteed, that a slight contamination of ilmenite by Fe^{3+} originated from the neighbouring magnetite. This problem was caused by the very small width of the analyzed ilmenite lamellae (mostly $< 2 \mu\text{m}$).

Equilibrium temperatures and oxygen fugacities were estimated via an interactive program (Ghiorso & Evans, 2008). This new model forms the basis of a revised FeTi-oxide geothermometer/oxygen barometer, which is applied to a newly compiled dataset of natural two oxide pairs from silicic volcanic rocks (Ghiorso & Evans, 2008). The recalculation of $\text{Fe}^{3+}/\text{Fe}^{2+}$ and totals with corrected iron as in Carmichael (1967), the calculation of molecular fractions using the four different models of Carmichael (1967); Anderson (1968); Lindsley & Spencer (1982) and Stormer (1983) was obtained by ILMAT software; the Magnetite-Ilmenite Geothermobarometry Program (Lepage, 2003).

The UTHSCSA Image Tool version, 2.01 Alpha 4 was used to generate digital images from the BSE pictures (e.g., Petřík et al., 2003) and to calculate the ilmenite/magnetite area ratios. The number of binary segments used varied between 10 and 15 for each sample, depending on the suitability of the BSE images and the appropriate Fe–Ti oxide textures (trellis-sandwich type). The applied conditions have been defined by authors, and therefore they should be considered with subjective cognition.

4. RESULTS

4.1. Distribution and textures of Fe–Ti oxides

Iron-titanium oxides represented by magnetite with ilmenite, rutile, and hematite exsolutions occur as irregular aggregates, up to 0.5 mm in size with a coexisting accessory mineral assemblage of zircon, monazite-(Ce), and xenotime-(Y). Moreover, gasparite-(Ce), chernovite-(Y), arsenian xenotime-(Y), and arsenian thorite also occur in the rhyolite from Tisovec-Rejkovo (Ondrejka et al., 2007).

Large Fe–Ti phenocrysts occur in the Tisovec rhyolite (up to 1.5 vol. %), and in the rhyolite at the Telgárt locality (up to 0.6 vol. %). The amount of the matrix or recrystallized former glass is similar in both occurrences (up to 89.6 vol. %). The rhyolites contain no biotite. The concentrations of K-feldspar vary from 0.5 to 6.5 vol. % in the Tisovec and Telgárt localities, respectively.

A broad survey of the Fe–Ti oxide textures and assemblages commonly encountered in the A-type rhyolites of the Silicic Superunit are shown in Fig. 2. Most of these depict a typical

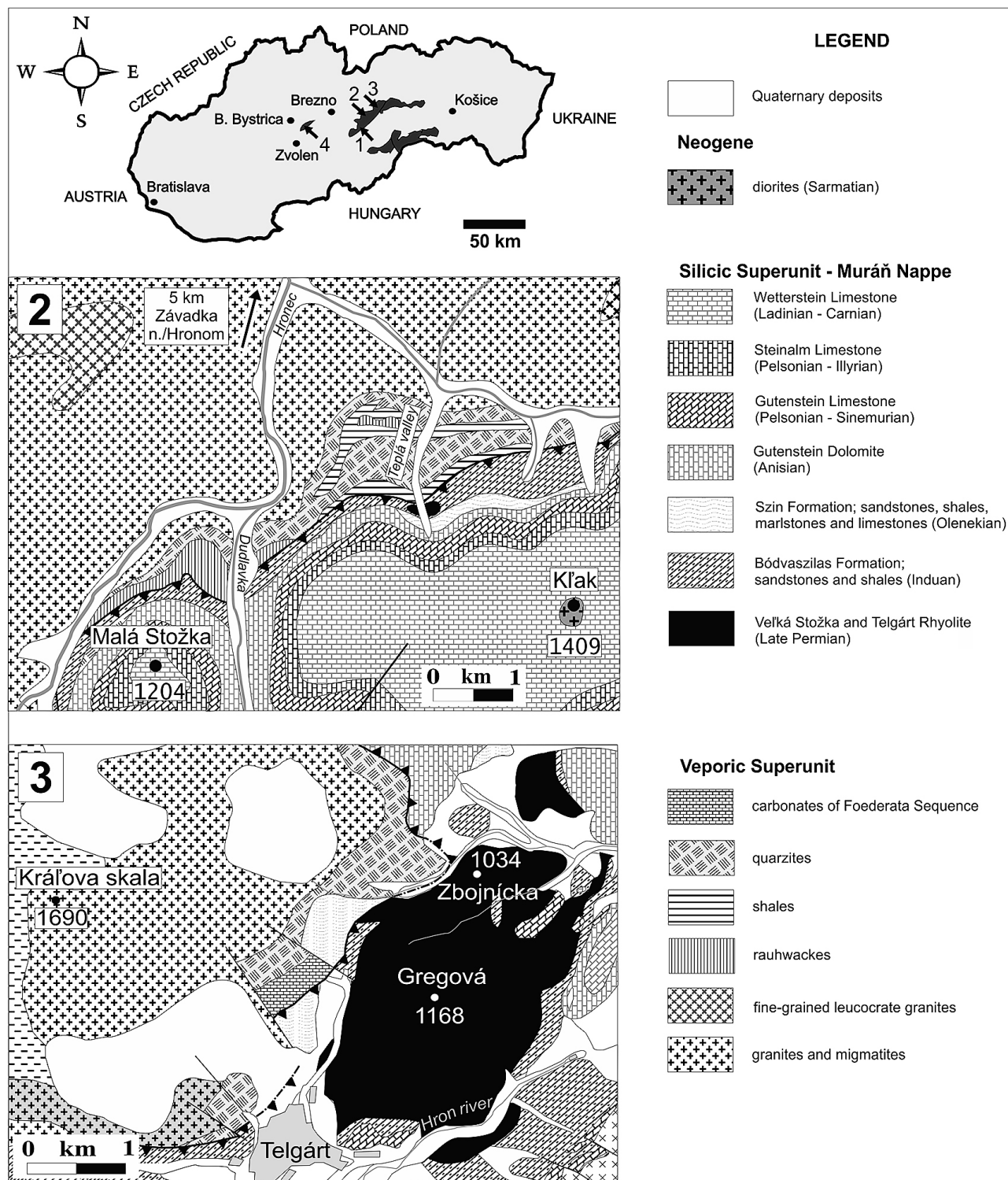
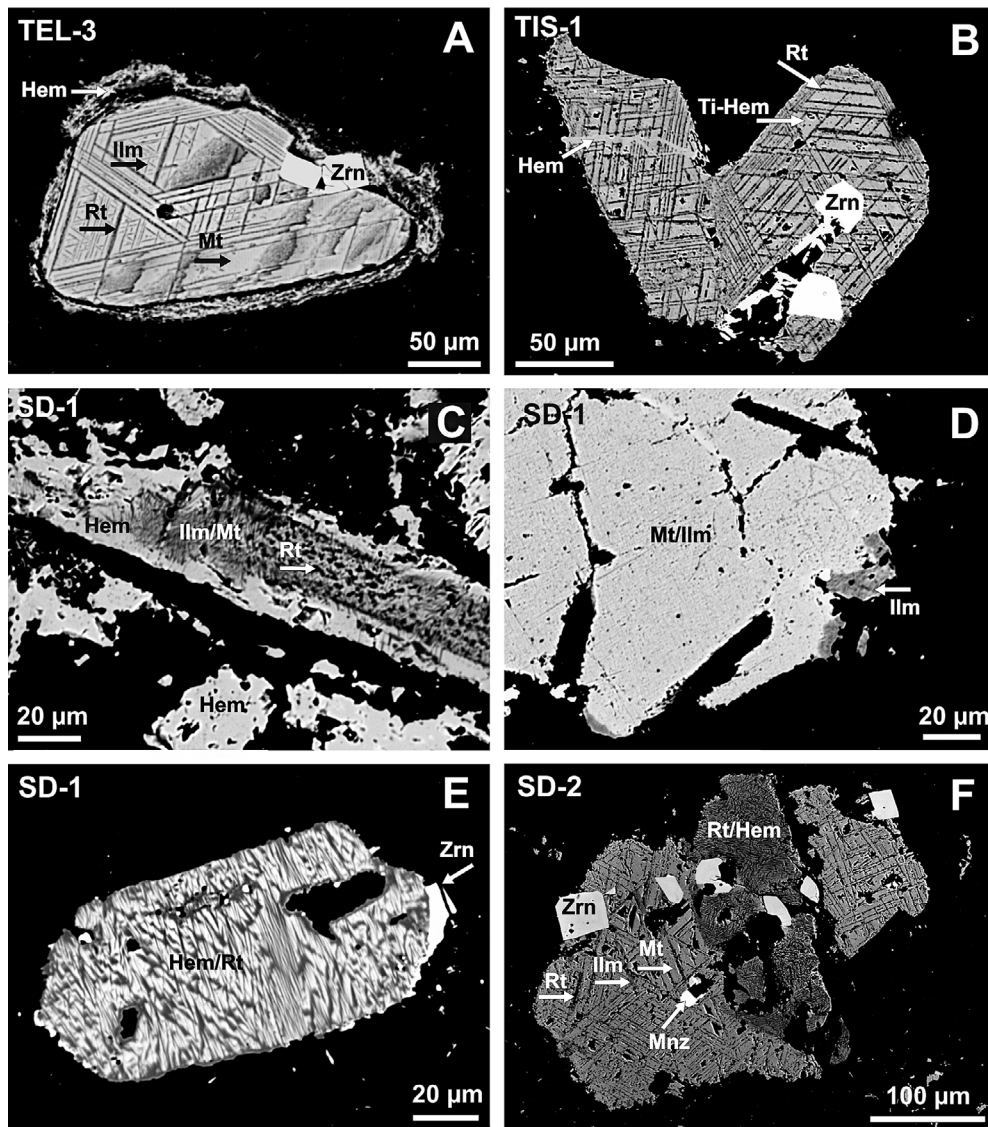


Fig. 1: Schematic map of Slovakia with the position of the Silicic Superunit (grey) and approximate positions of Lower Triassic volcanics: 1 – Tisovec–Rejkovo; 2 – Veľká Stožka–Dudlavka (detailed geological map after Klinec, 1976); 3 – Telgárt–Gregová (detailed geological map after Klinec, 1976); 4 – Poniky–Drienok. For further details of locality 1 and 4 see Uher et al. (2002) and Ondrejka et al. (2007).

Obr. 1: Schematická mapa Slovenska s pozíciou tektonickej jednotky silicika (šedá) a približnou pozíciou spodnotriasových vulkanitov: 1 – Tisovec–Rejkovo; 2 – Veľká Stožka–Dudlavka (detailná geologická mapa podľa Klinca, 1976); 3 – Telgárt–Gregová (detailná geologická mapa podľa Klinca, 1976); 4 – Poniky–Drienok. Pre detailnejšie informácie o lokalitách 1 a 4 pozri Uher et al. (2002) a Ondrejka et al. (2007).

Fig. 2. Back scattered electron images (BSE) of iron-titanium oxides from the A-type rhyolites in the Silicic Superunit. **A:** Deuteric oxidation "oxyexsolution" of primary Ti-rich magnetite (sandwich type). Thin ilmenite (Ilm) and thick rutile (Rt) "sandwich" laths with uniform sides and with secondary and tertiary trellis sets along {111} spinel planes in the host magnetite (Mt). Zircon (Zrn) is the most abundant accessory mineral enclosed in Fe-Ti oxides. The outer rim is represented by hematite (Hem). Sample TEL-3: Telgárt-Gregová. **B:** The progressive decomposition (C4 (?) stage) of primary Ti-rich magnetite to ferrian rutile (Rt) and Ti-rich hematite (Ti-Hem) trellis lamellae with a secondary hematite vein (Hem) and enclosed zircon (Zrn). Sample TIS-1: Tisovec-Rejkovo. **C:** Very fine trellis of ilmenite/magnetite (Ilm/Mt) lamellae with rutile inclusions (Rt) in the Ti rich central part of the grain enclosed in hematite (Hem). Sample SD-1: Veľká Stožka-Dudlavka. **D:** Fine trellis of magnetite/ilmenite (Mt/Ilm) lamellae, most likely due to the very rapid oxidation of primary titanomagnetite with an external composite inclusion of ilmenite (Ilm) having a



well-developed sharp boundary along the magnetite/ilmenite aggregate. Sample SD-1: Veľká Stožka – Dudlavka. **E:** A complete decomposition of primary Ti-rich magnetite to a very fine lamellae aggregate of hematite/rutile (Hem/Rt) with very thin residual ilmenite boundaries along the hematite – rutile crystals, most likely as the result of ilmenite breakdown to rutile and hematite. Sample SD-1: Veľká Stožka – Dudlavka. **F:** The central grain represents the breakdown of ilmenite to rutile with a co-existing hematite aggregate (Rt/Hem). Marginal grains are representative of the deuteric oxidation of primary Ti-magnetite to ilmenite (Ilm) laths oriented along {111} magnetite planes, accompanied in some places by a progressive decomposition to rutile (Rt). Accessory minerals are represented by zircon (Zrn) and monazite (Mnz) enclosed in Fe-Ti oxide aggregates. Sample SD-2: Veľká Stožka–Dudlavka.

Obr. 2. Obrázky späťne rozptýlených elektrónov (BSE) Fe-Ti oxidov z rhyolitov A-typu silicika **A:** Deuterická oxidácia "oxyexsolúcia" primárneho Ti bohatého magnetitu (sendvičový typ). „Sendvičové“ lamely tenkého ilmenitu (Ilm) a hrubého rutilu (Rt) vytvárajúce sieťový vzor pozdĺž spinelových plôch {111} v hostiteľskom magnetite (Mt). Zirkón (Zrn) je najhojnejší akcesorický minerál uzatvorený v Fe-Ti oxidoch. Okrajový lem je tvorený hematitom (Hem). Vzorka TEL-3: Telgárt-Gregová. **B:** Pokročilý rozklad (C4? štádium) primárneho Ti bohatého magnetitu na Fe rutil (Rt) a Ti bohatý hematit (Ti-Hem) vytvárajúce mriežkový vzor so sekundárnou hematitovou žilkou (Hem) a uzatvoreným zirkónom (Zrn). Vzorka TIS-1: Tisovec-Rejkovo. **C:** Veľmi jemné lamely ilmenitu/magnetitu (Ilm/Mt) s inklúziami rutilu (Rt) v centrálnej, Ti bohatej časti zrna uzatvoreného v hematite (Hem). Vzorka SD-1: Veľká Stožka–Dudlavka. **D:** Jemnozrné lamely magnetitu/ilmenitu (Mt/Ilm), ktoré sú pravdepodobne produktom veľmi rýchlej oxidácie primárneho titanomagnetitu s externou inklúziou ilmenitu (Ilm) s ostrým kompozičným rozhraním pozdĺž agregátu magnetitu/ilmenitu. Vzorka SD-1: Veľká Stožka – Dudlavka. **E:** Kompletne rozložený primárny Ti bohatý magnetit na jemnozrný lamelárny agregát hematitu/rutilu (Hem/Rt) s veľmi jemnozrným reziduálnym lemom ilmenitu pozdĺž kryštálov hematitu a rutilu, ktoré sú pravdepodobne produktom rozpadu ilmenitu na rutil a hematit. Vzorka SD-1: Veľká Stožka – Dudlavka. **F:** Centrálné zrna reprezentujú rozpad ilmenitu na rutil s koexistujúcim agregátom hematitu (Rt/Hem). Okrajové zrna reprezentujú deuterickú oxidáciu primárneho Ti-magnetitu na ilmenitové lamely (Ilm) orientované pozdĺž magnetitových plôch {111} a sprevádzané na niektorých miestach progresívnym rozpadom na rutil (Rt). Akcesorické minerály sú zastúpené zirkónom (Zrn) a monazitom (Mnz) uzatvorených v agregátoch Fe-Ti oxidov. Vzorka SD-2: Veľká Stožka–Dudlavka.

trellis-sandwich type texture: lamellae of ilmenite along the {111} planes of the host magnetites as a result of "oxidation-exsolution" or "oxyexsolution" (Buddington & Lindsley, 1964) of the ulvöspinel component from a high temperature Ti-rich magnetite ("titanomagnetite") solid solution (Fig. 2A,B) suitable for geothermometry. In some places a very tiny trellis of ilmenite/magnetite lamellae (Fig. 2C), or composite type of ilmenite_{ss} intergrowth occurs (Fig. 2D) with complete decomposition of primary Ti-rich magnetite to a very fine lamellae aggregate of hematite/rutile (Fig. 2E). The progressive decomposition to Fe-rich rutile/hematite (the C4 stage according to Haggerty's, 1991 definition) is less common (Fig. 2B,F). This type of texture most likely represents the final stage of the Fe-Ti oxide cooling evolution.

4.2. Iron-titanium oxides compositional data

Representative compositions of Fe-Ti oxide minerals from the investigated rhyolites are shown in Table 1. The ulvöspinel component (Fe₂TiO₄) in oxyexsolved magnetite lamellae close to the end-member shows a composition ranging from 3 to 18 mol. %, a galaxite component (MnAl₂O₄) is up to 4.6 mol. % and a hercynite component (FeAl₂O₄) up to 3 mol. %. Trace components in the magnetite host, such as Cr₂O₃, MgO and NiO represent less than 0.1 wt. % in most of the analyzed crystals, and apparently, they are not significant constituents.

The oxyexsolved ilmenite lamellae are very thin (up to 4 μm, mostly <2 μm) and they contain of 0.6 to 35 mol. % of the hematite component; up to 3 mol. % of the pyrophanite component (MnTiO₃), and up to 2 mol.% of the geikielite component (MgTiO₃).

Compositional variation in the hematite, which are considered to be the result of the final oxidation of ilmenite and hematitization (maghemitization?) of magnetite, show considerable solid solution with the ilmenite component, reaching up to 40 mol. %. On the other hand, the concentration of the pyrophanite component (MnTiO₃) is low (1.6 mol. %) and other trace oxides, such as Cr₂O₃ and MgO represent less than 0.3 wt. % in most of the analyzed crystals, and apparently, they are also not significant constituents (Table 1; Fig. 3).

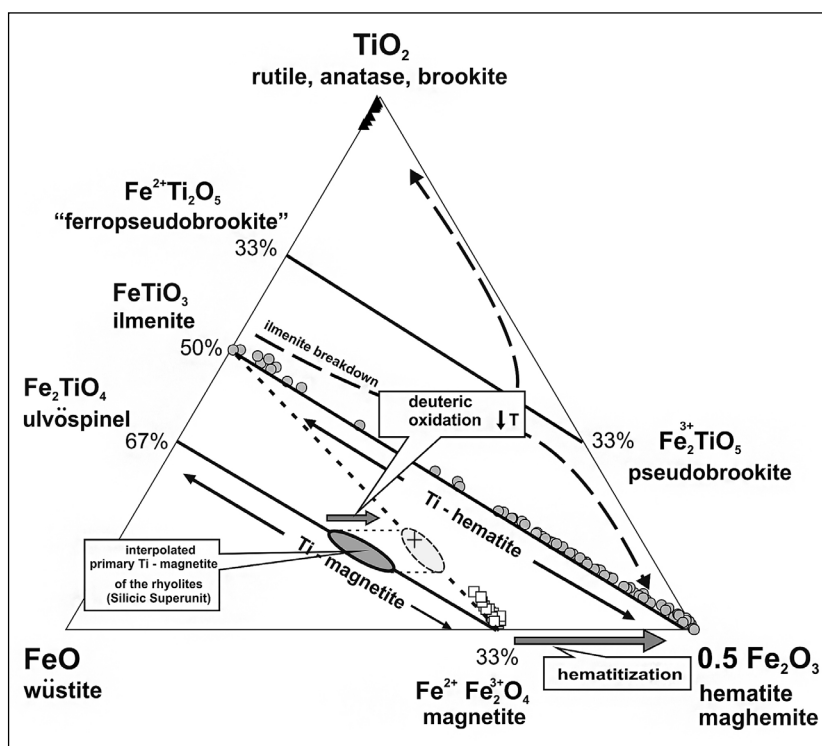
The rutile composition is uniform in all samples and is very close to the ideal TiO₂ end-member. However, in some cases the Fe-rich rutile is observed to have a slight enrichment in Fe (up to 5.1 wt. % of FeO, 0.057 apfu Fe; Table 1). Such rutile is in coexistence with hematite from the C4(?) stage (Fig. 2B). Other minor constituents, such as Al₂O₃, Cr₂O₃, MnO, and MgO represent less than 0.1 wt. % for most of the analyzed crystals.

Fe-Ti oxide compositions are plotted on a TiO₂-FeO-Fe₂O₃ ternary diagram (Fig. 3). Analyses of deuteritic oxidation products are plotted along the magnetite-ilmenite tie line, while secondary phases are represented by points along the ilmenite-hematite line ("titanohematites") and in the proximity of TiO₂ vertex.

Fig. 3. The composition of Fe-Ti oxides plotted in TiO₂-FeO-0.5Fe₂O₃ ternary diagram (atomic proportions). Thick lines denote high temperature solid solutions (ulvöspinel - magnetite, hematite - ilmenite, pseudobrookite - ferropseudobrookite); the dashed line shows a heterostructural tie line ilmenite - magnetite as the result of deuteritic oxidation and breakdown of primary Ti-rich magnetite. The Cross mark represents the average composition; dashed ellipse represents the range of magnetite/ilmenite compositions calculated using the mixing equation (Appendix). The thick ellipse represents these compositions interpolated to the ulvöspinel - magnetite line. Minor components are allocated as follows: FeO=ΣR²⁺=Fe²⁺+Mg+Mn; Fe₂O₃=0.5ΣR³⁺=0.5(Fe³⁺+Al+Cr). Using (1/2)Fe₂O₃ as the parameter for the Fe³⁺ corner normalizes the diagram to one cation, producing the convenient effect that lines of oxidation (increasing the Fe³⁺:Fe²⁺ ratio) are parallel to the base of the diagram.

Obr. 3. Zloženie Fe-Ti oxidov vyjadrené v TiO₂-FeO-0,5Fe₂O₃ trojuholníkovom diagrame (apfu). Hrubé čiary reprezentujú vysokotepelné tuhé roztoky (ulvöspinel - magnetit,

hematit - ilmenit, pseudobrookit - ferropseudobrookit); prerušované čiary predstavujú heteroštruktúrnú líniu medzi ilmenitom a magnetitom ako výsledok deuteritickej oxidácie a rozpadu primárneho Ti bohatého magnetitu. Krížik reprezentuje priemerné zloženie, prerušovaná elipsa rozsah zloženia magnetitu/ilmenitu vypočítaného pomocou zmiešavacej rovnice (Appendix). Hrubá elipsa reprezentuje interpolované zloženie na líniu ulvöspinel - magnetit. Obsahy minoritných oxidov sú rozdelené nasledovne FeO=ΣR²⁺=Fe²⁺+Mg+Mn; Fe₂O₃=0,5ΣR³⁺=0,5(Fe³⁺+Al+Cr). Použitie (1/2)Fe₂O₃ ako parametra pre vrchol trojuholníka Fe³⁺ normalizuje diagram na 1 katión, čo má efekt na pozíciu oxidačnej línie (zvyšovanie pomeru Fe³⁺:Fe²⁺), ktorá je rovnobežná so základňou diagramu.



Tab. 1: Representative microprobe analyses of iron-titanium oxides from the A- type rhyolites of the Silicic Superunit. The equilibration temperature and fO_2 values are referenced below each magnetite/ilmenite pair (as in geothermometer usage by Ghiorso & Evans, 2008). FeO and Fe_2O_3 were calculated after Carmichael (1967). Average magnetite: n=29; average ilmenite: n=35; titanomagnetite average composition was recalculated by the mixing equation (Appendix). Mineral abbreviations: AVG Mt – average magnetite, AVG Ilm – average ilmenite, Mt – magnetite, Hem – hematite, Ilm – ilmenite, Rt – rutile, cTMt – calculated titanomagnetite, n.a. = not analysed.

Tab. 1: Reprezentatívne mikrosondové analýzy Fe-Ti oxidov z rhyolitov A-typu silicika. Teploty ekvibrácie a hodnoty fO_2 sú uvedené pri každom magnetit/ilmenit páre (použitý geotermometer Ghiorso & Evans, 2008). FeO a Fe_2O_3 boli počítané podľa Carmichael (1967). Priemerný magnetit: n=29, priemerný ilmenit: n=35, priemerné zloženie titanomagnetitu bolo vypočítané na základe zmiešavacej rovnice (Appendix). Skratky minerálov: AVG Mt – priemerný magnetit, AVG Ilm – priemerný ilmenit, Mt – magnetit, Hem – hematit, Ilm – ilmenit, Rt – rutil, cTMt – vypočítaný titanomagnetit, n.a. = neanalyzované.

mineral	Mt	Ilm	Mt	Ilm	Mt	Ilm	Hem	Hem	Hem	Rt	Rt	AVG Mt	AVG Ilm	cTMt
locality	Telgárt		Tisovec		V. Stožka		Telgárt	Tisovec	V. Stožka	Poniky	V. Stožka	Telgárt		
sample	TEL-1		TIS-1		SD-1		TEL-1	TIS-1	SD-1	PO-6	SD-1	TEL-1		
TiO ₂	4.37	43.76	1.45	48.97	3.66	40.03	16.07	12.21	5.53	98.41	93.59	2.88	46.90	17.65
Al ₂ O ₃	0.91	0.57	0.46	0.46	0.46	0.21	1.12	0.16	0.97	0.10	0.08	0.68	0.47	0.61
Cr ₂ O ₃	0.02	0.03	0.03	0.01	0.05	0.03	0.00	0.00	0.02	0.00	0.03	0.02	0.02	0.02
Fe ₂ O ₃	58.40	14.20	66.11	2.90	59.97	21.80	68.34	76.12	88.66			61.20	6.50	49.21
FeO	34.35	38.30	30.45	41.98	33.27	34.62	13.94	10.88	4.75	1.66	5.06	32.42	40.88	29.53
MnO	0.25	0.55	0.27	1.47	0.60	1.13	0.31	0.08	0.16	0.03	0.15	0.62	0.76	0.67
MgO	0.10	0.29	0.00	0.33	0.02	0.14	0.12	0.01	0.04	0.00	0.39	0.10	0.30	0.17
NiO	0.05	0.00	0.00	0.00	0.00	0.06	n.a.	n.a.	n.a.	n.a.	n.a.	0.02	0.00	0.01
Sum	98.45	97.70	98.77	96.12	98.02	98.00	99.89	99.47	100.12	100.20	99.30	97.94	95.83	97.88
Formulae based on 2 oxygens (rutile), 2 cations (ilmenite, hematite) and 3 cations (magnetite)														
Ti ⁴⁺	0.127	0.853	0.042	0.964	0.107	0.783	0.314	0.242	0.109	0.990	0.990	0.085	0.928	0.520
Al ³⁺	0.041	0.017	0.021	0.014	0.021	0.006	0.034	0.005	0.030	0.002	0.001	0.031	0.015	0.028
Cr ³⁺	0.001	0.001	0.001	0.000	0.002	0.001	0.000	0.000	0.000	0.000	0.000	0.001	0.000	0.001
Fe ³⁺	1.703	0.277	1.896	0.057	1.762	0.426	1.640	1.750	1.856	0.019	0.059	1.799	0.129	1.451
Fe ²⁺	1.113	0.828	1.031	0.919	1.087	0.753						1.059	0.899	0.968
Mn ²⁺	0.008	0.012	0.009	0.033	0.020	0.025	0.007	0.002	0.003	0.000	0.002	0.020	0.017	0.022
Mg ²⁺	0.006	0.011	0.000	0.013	0.001	0.005	0.004	0.000	0.001	0.000	0.008	0.006	0.012	0.010
Ni ²⁺	0.001	0.000	0.000	n.a.	0.000	0.001	n.a.	n.a.	n.a.	n.a.	n.a.	0.001	0.000	0.000
Catsum	3.000	2.000	3.000	2.000	3.000	2.000	2.000	2.000	2.000	1.011	1.061	3.000	2.000	3.000
X _{galaxite}	0.008		0.009		0.018							0.019		0.017
X _{ulvöspinel}	0.119		0.041		0.100							0.079		0.406
X _{hercynite}	0.019		0.010		0.010							0.015		0.011
X _{magnetite}	0.849		0.940		0.870							0.881		0.560
X _{geikielite}		0.010		0.012		0.004	0.003	0.000	0.001				0.011	
X _{ilmenite}		0.734		0.871		0.623	0.184	0.137	0.056				0.853	
X _{pyrophanite}		0.011		0.031		0.021	0.004	0.001	0.002				0.016	
X _{hematite}		0.245		0.086		0.352	0.810	0.862	0.941				0.120	
T (°C)		657		402		655								
log ₁₀ fO_2 (relative to NiNiO)		1.09		0.29		1.53								
log fO_2		-17.44		-27.28		-15.97								

4.3. Fe–Ti oxide geothermometry

The estimation of equilibration temperatures and oxygen fugacities were obtained for Tisovec – Rejkovo (TIS), Veľká Stožka

– Dudlavka (SD) and Telgárt – Gregová (TEL) samples only. The Poniky – Drienok sample was excluded due to unsuitable chemical composition of ilmenite-magnetite pairs. However, the compositional data on ilmenite-hematite_{ss} and rutile phases are

plotted in general ternary diagram (Fig. 3) and following calculation of T-fO₂ has been done using parameters from Ghiorso & Sack (2008).

The Telgárt rhyolite displays a range of equilibration temperatures (750–550 °C) and the oxygen fugacity values approximate the NiNiO (nickel-nickel oxide) buffer ranging from $-0.76 \Delta \log fO_2$ (~418 °C) to $1.09 \Delta \log fO_2$ (~657 °C). The equilibration temperatures estimated for the Velká Stožka rhyolite are generally lower 660–430 °C and oxygen fugacity values also approach the NiNiO buffer by ranging from $-0.75 \Delta \log fO_2$ (~600 °C) to $1.53 \Delta \log fO_2$ (~655 °C). The equilibration temperatures estimated for the Tisovec – Rejkovo rhyolite are similar (620–400 °C) but their oxygen fugacity values follow the NiNiO buffer with minimal deviations ranging from $-0.52 \Delta \log fO_2$ (~600 °C) to $0.21 \Delta \log fO_2$ (~532 °C) as shown in Fig. 4.

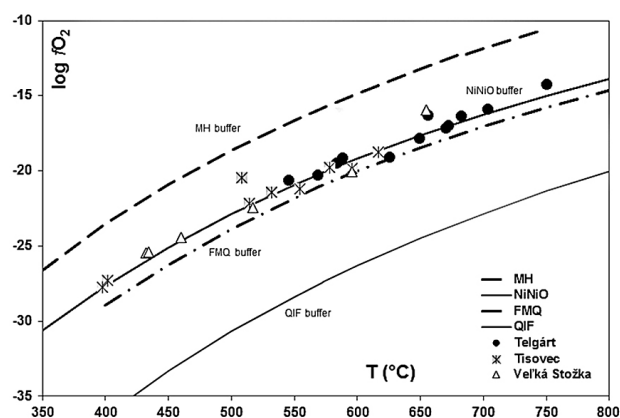


Fig. 4. The equilibration temperature and fO_2 estimated from Fe–Ti oxides in the A-type rhyolites of the Silicic Superunit, showing a decrease in the oxygen fugacity during cooling. Applied fugacity buffers curves: Quartz–Iron–Fayalite (QIF), Fayalite–Magnetite–Quartz (FMQ), Nickel–Nickel–Oxide (NiNiO) and Magnetite–Hematite (MH) as calculated after Frost, (1991^a). Equilibrium temperatures and fugacities calculated after Ghiorso & Evans (2008).

Obr. 4. Rovnovážna teplota a hodnota fO_2 stanovená z Fe–Ti oxidov v rhyolitoch A- typu silicika poukazuje na pokles fugacity kyslíka počas chladnutia. Použité fugacitné bufre: Kremeň–Železo–Fayalit (QIF), Fayalit–Magnetit–Kremeň (FMQ), Nikel–Nikel–Oxid (NiNiO) a Magnetit–Hematit (MH), vypočítané podľa Frost, (1991^a). Rovnovážne teploty a fugacity vypočítané podľa Ghiorso & Evans (2008).

5. DISCUSSION AND CONCLUSIONS

5.1. Compositional variability of Fe–Ti oxides

Iron-titanium oxides represented by magnetite with ilmenite, rutile and hematite exsolutions represent the only dark accessory phases in the investigated A-type rhyolites from the Silicic Superunit. The compositional variations of the Fe–Ti oxides reflect the character of A-type chemistry of the rhyolites, therefore minor constituents Cr₂O₃, MnO, MgO and NiO are not present in significant amounts (Table 1). The effects of incorporated minor impurities, which are usually present up to

a few percent in natural Fe–Ti oxides, were discussed e.g. by Nagata (1961). However the incorporation of Fe and Ti as major cations is reflected according to the crystallographic rules of both isostructural solid solution series (ulvöspinel – magnetite with an inverse spinel structure and hematite – ilmenite with a rhombohedral structure). The widest range of Fe–Ti miscibility in the studied samples is presented along the ilmenite-hematite join, where the significant hematite component in ilmenite from silicic volcanic rocks was also documented (Frost & Lindsley, 1991; Butler, 1992).

The recalculated primary composition of average Ti-rich magnetite (Appendix) shows the slight predominance of magnetite (0.56 mol. %) component over ulvöspinel (0.41 mol. %) – (Table 1). However, Fe–Ti oxides in felsic rocks often have low Ti contents and primary magnetites are Ti-poor and close to end member of magnetite (Butler, 1992), especially those late magmatic (Broska & Petřík, 2011). On the other hand, Fe–Ti oxides in some silicic volcanics show a wider range in titanium contents ranging from Usp₁₀₀ (fayalite rhyolites) to Usp₁₀ (more oxidized rhyolites with biotite and hornblende) – (Frost & Lindsley, 1991). Although primary Ti-rich magnetites of intermediate composition are common, intermediate Ti-rich hematites are relatively rare (Butler, 1992). The recalculated composition of primary Fe–Ti oxide phase suggests the slight oxidized nature of the rhyolite.

The incorporation of Fe into rutile (Table 1) is limited at low temperatures and can be explained by charge-coupled substitutions $2M^{5+} + Fe^{2+} = 3Ti^{4+}$, or $Fe^{3+} + M^{5+} = 2Ti^{4+}$, where M can be V, Nb, Ta or Sb (Waychumas, 1991). Unfortunately, the M³⁺ cations are below the detection limit in these rutiles. Rutile which formed at moderate temperatures may also contain a small amount of Fe³⁺ which is observed as hematite exsolutions (Putnis, 1978). The nature of this defective solution is unclear, but as elevated temperatures are required for significant Fe³⁺ solubility (3 % at 1400 °C) the presence of charge-compensating stacking faults and cation or anion vacancies is likely (Waychumas, 1991).

5.2. Re-equilibration of Fe–Ti oxides and geothermometry

Assemblages and compositions of iron-titanium oxides are important in the estimation of oxygen fugacity and the equilibrium temperature during evolution of these magmatic rocks. Generally, a high oxygen fugacity in the magmatic system is resulted in the occurrence of ilmenite, magnetite and hematite, whereas the presence of hematite indicates the highest oxygen fugacity which can be reached in a common acid rock (Frost & Lindsley, 1991)

The high temperature ulvöspinel – magnetite solid solution Ti_{1-x}Fe_{3-x}O₄ (known as titanomagnetites) is the most fundamental Fe–Ti phase, particularly in igneous rocks (Nagata, 1961). Titanium-rich magnetite can be oxidized or reduced by a variety of processes (O'Reilly, 1984) and therefore its composition can be recalculated from its product minerals (Saito et al., 2004), which is represented by magnetite with ilmenite lamellae in the mixing equation (c.f. Appendix, Table 1). An idealized Ti-rich magnetite composition results from the reverse process of

pure deuteric oxidation/subsolidus exsolution. This can easily be interpolated onto the ulvöspinel – magnetite line (Fig. 3).

Ferromagnetic Ti-rich magnetite undergoes extensive subsolidus re-equilibration during cooling. According to Frost et al. (1988), the general re-equilibration of Fe–Ti oxides involves three different processes: (1) oxide-silicate re-equilibration; (2) interoxide re-equilibration; and (3) intraoxide re-equilibration. Titanium in Ti-rich magnetite is exhausted during intra-oxide re-equilibration in a reaction forming ilmenite, thus at lower temperatures, compositional gaps develop and the intermediate compositions unmix or exsolve into Ti-rich regions and Ti-poor regions by solid state diffusion of Fe and Ti cations (Butler, 1992). This process produces the typical texture of ilmenite lamellae within magnetite (Fig. 2A) and it has been called “oxyexsolution” (Buddington & Lindsley, 1964). This process is described by the following chemical reaction (Rollinson, 1980; Frost, 1991^b):

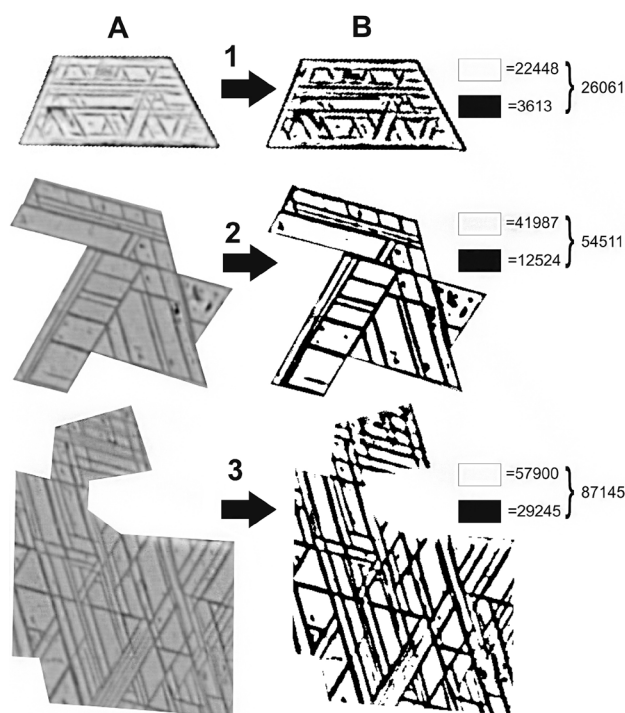
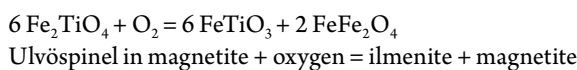
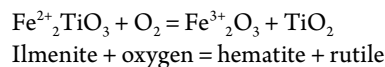


Fig. 5. Representative examples of BSE images (A) with magnetite (bright) and ilmenite (dark) lamellae converted to binary images (B) with magnetite (white) and ilmenite (black). Representative polygons (sample TEL-3) have variable angles and strictly defined sharp boundaries and well-developed magnetite and ilmenite pairs. Note: All values are in pixels (square units), and the binary images are generated by UTHSCSA Image Tool software.

Obr. 5. Reprezentatívne príklady BSE obrázkov s lamelami (A) magnetitu (svetlé) a ilmenitu (tmavé) konvertované na binárne obrázky lamiel (B) magnetitu (biele) a ilmenitu (tmavé). Reprezentatívne polygóny (vzorka TEL-3) majú rôzne uhly, jasne definované a ostré rozhrania a dobre vyvinuté magnetitové a ilmenitové páry. Poznámka: Všetky hodnoty sú v pixeloch (plošných jednotkách) a binárne obrázky sú vytvorené v počítačovom programe UTHSCSA Image Tool.

The magnetite-ilmenite oxybarometer-thermometer calibrated by Ghiorso & Evans (2008) describe the initial oxidation conditions and initial temperature to be about 620 °C for Tisovec – Rejkovo, 660 °C for Veľká Stožka, and 750 °C for Telgárt (Fig. 5). Re-equilibration processes during cooling and subsequent fluid activity result in the formation of rutile and hematite (Fig. 2B) from ilmenite according to the following reaction (e.g., Deer et al., 1982):



The formation of rutile is considered to be the final stage for primary Ti-rich magnetite decomposition or ilmenite decomposition with accompanying hematite. The formation of titanite is a normal final stage in Ca-rich metamorphic rocks (Harlov et al., 2006) and intermediate to acid magmatic rocks (Broska et al., 2007). It is not developed in these rocks, due to the absence of Ca in the A-type rhyolites (cf. Uher et al., 2002).

Magnetite-ilmenite oxide barometry-thermometry of A-type rhyolites reveals a relatively smooth evolutionary trend in the late-magmatic/high-temperature hydrothermal or subsolidus/solidus stages. This trend reflects the rapid cooling of volcanic rocks in comparison with the low grade metamorphism of acid plutonic rocks (e.g., Rollinson, 1980).

At higher oxygen fugacities buffered in the FMQ reaction, Fe is present in both oxidation states as ferrous (divalent) and ferric (trivalent) ion and is mainly incorporated into magnetite at the expense of the silicates (Frost, 1991^a). The relatively higher values of oxygen fugacity during the rhyolites late magmatic/subsolidus evolution to postmagmatic alteration is supported by the presence of accessory strontian barite and rarely cerianite-(Ce) in the Tisovec-Rejkovo rhyolitic body (Ondrejka et al., 2007). Moreover, the calculation of equilibrium temperatures for A-type rhyolites (400–750 °C) are lower than previous orthomagmatic temperature values in range of 800–900 ± 50 °C estimated from the zircon typology (cf. Pupin, 1980) and zircon saturation temperature (820–895 °C) as calculated from the bulk-rock chemical composition (cf. Watson & Harrison, 1983). These temperatures indicate that the rhyolites originated from a hot and dry magma (Uher et al., 2002; Ondrejka, 2004), while Fe–Ti oxide thermometry based on intra-oxide re-equilibration between spinel and rhombohedral oxide pairs (e.g., Ghiorso & Evans, 2008) reflects the conditions during subsequent subsolidus/solidus cooling history of a rock. Surely the lowest temperatures obtained from the two-oxide geothermometer (Fig. 4) are unrealistic because they fall below the expected solidus of rhyolitic magma.

5.3. Source of the Fe- rich rhyolite

Although the mobility of Fe in high temperature brines derived from rhyolites can be significant (Simon et al., 2004), the high concentration of scattered magnetite in the host rhyolite rock is not due to hydrothermal precipitation because of the high amount of primary Ti in the majority of the present magnetite. On the other hand, part of hematite forming rims on magnetite

and veins in host rock (Fig. 2) most likely originated during high temperature late/post-magmatic activity. Hypergene processes contributed to the increased Fe/Ti ratio as well. An evolved Fe concentration (high Fe/Mg ratio) is a common phenomenon of A-type melts (cf. Whalen et al., 1987; Sylvester, 1989, 1994), and the high amount of Fe–Ti oxides is a product of such primary iron melt enrichment. A-type rhyolitic volcanic rocks are highly enriched in iron, but also in HFSE, including REE and depleted in Ca, Mg, Sr (e.g., Uher et al., 2002; Samuel, et al. 2007).

The relatively low abundance of phenocrysts in A-type rhyolites (~10 vol. %) suggests that the magma did not remain in a shallow storage chamber for a long time (Smith et al., 2005). Usually, a hot and dry rhyolite melt contains low amounts of phenocrysts as it is known for instance from Cenozoic volcanic centres in the Western Cordillera in USA (Christiansen & McCurry, 2008). Here, the rhyolites show a relatively wide equilibration temperature range from ~750 to ~400 °C. Some rift-related rhyolites with A-type affinity also record relatively low temperatures of equilibration (≤ 700 °C) and low fO_2 ($\leq FMQ$) (MacDonald & Scaillet, 2006). The conditions observed in Tisovec, Telgárt and Veľká Stožka localities exhibit similar conditions in spite of intraplate Permian evolution within Pangea continent.

The overall mineralogical and chemical characteristics of studied rhyolites resulted from intraplate geotectonic setting (Uher et al., 2002). Partial melting of rift-related deep crustal rocks and asthenospheric upwelling provided the mechanism for rhyolite magma origin and subsequent lithospheric extension and crustal fracturing triggered the eruption of these magmas. Volatiles from the upper mantle were important agents for heat transfer sufficient for the enhanced anatexis of crustal rocks (Samuel, et al. 2007). The character of eruption is probably consistent with the Peléan type of eruption in a small water volume (Martel et al., 1998).

Acknowledgement: This work was supported by the Slovak Research and Development Agency under the contract No. APVV-0081-10 and VEGA Agency No. 1/0257/13 and 1/0079/15. The authors thank Patrik Konečný from the D. Štúr Geological Institute in Bratislava, and also Dan Topa from the Salzburg University for providing microprobe analyses, Peter Tropper, Monika Huraiová, Jaroslav Pršek and Rastislav Vojtko (AGEOS editor) for helpful comments and recommendations. We also thank Ray Marshall for English language review.

6. REFERENCES

- Anderson A.T., 1968: Oxidation of the LaBlanche Lake titaniferous magnetite deposit, Quebec. *Journal of Geology*, 76, 5, 528–547.
- Andersen D.J. & Lindsley D.H., 1985: New (and final!) models for the Ti magnetite/ilmenite geothermometer and oxygen barometer. *Abstract AGU 1985 Spring Meeting Eos Transactions. Am. Geophys. U.* 66, 18, 416.
- Broska I, Harlov D., Tropper P. & Siman P., 2007: Formation of magmatic titanite and titanite-ilmenite phase relations during granite alteration in the Tribeč Mountains, Western Carpathians, Slovakia. *Lithos*, 95, 1–2, 58–71.
- Broska I. & Petrik I., 2011: Accessory Fe-Ti oxides in the West-Carpathian I-type granitoids: witnesses of the granite mixing and late oxidation processes. *Mineralogy and Petrology*, 102, 1–4, 87–97.
- Buddington A.F., & Lindsley D.H., 1964: Iron-titanium oxide minerals and synthetic equivalents. *Journal of Petrology*, 5, 2, 310–357.
- Butler R.F., 1992: Paleomagnetism: Magnetic Domains to Geologic Terranes, Chapter 2. Ferromagnetic Minerals, Blackwell Scientific Publications, 16–30.
- Carmichael I.S.E., 1967: The iron-titanium oxides of salic volcanic rocks and their associated ferromagnesian silicates. *Contributions to Mineralogy and Petrology*, 14, 1, 36–64.
- Christiansen E.H. & McCurry M., 2008: Contrasting origins of Cenozoic silicic volcanic rocks from the western Cordillera of the United States. *Bulletin of Volcanology*, 70, 3, 251–267.
- Deer W.A., Howie R.A. & Zussman J., 1982: An introduction to the rock-forming minerals. Longman Scientific & Technical, London & New York, 696 pp.
- Demko R. & Hraško L., 2013: Ryolitové teleso Gregová pri Telgárte. *Mineralia Slovaca*, 45, 4, 161–174.
- Ewart A., Hildreth W. & Carmichael I.S.E., 1975: Quaternary acid magma in New Zealand. *Contributions to Mineralogy and Petrology*, 51, 1, 1–27.
- Frost B.R., 1991^a: Introduction to oxygen fugacity and its petrologic importance. In: Lindsley D.H. (Ed): Oxide minerals: Petrologic and magnetic significance. *Review in Mineralogy*, 25, 1–8.
- Frost B.R., 1991^b: Magnetic petrology: Factors that control the occurrence of magnetite in crustal rocks. In: Lindsley D.H. (Ed): Oxide minerals: Petrologic and magnetic significance. *Review in Mineralogy*, 25, 489–506.
- Frost B.R. & Lindsley D.H., 1991: Occurrence of iron-titanium oxides in igneous rocks. In: Lindsley D.H. (Ed): Oxide minerals: Petrologic and magnetic significance. *Review in Mineralogy*, 25, 433–462.
- Frost B.R., Lindsley D.H. & Andersen D.J., 1988: Fe-Ti oxide-silicate equilibria: assemblage with fayalitic olivine. *American Mineralogist*, 73, 7–8, 727–740.
- Ghiorso M.S. & Evans B.W., 2008: Thermodynamics of rhombohedral oxide solid solutions and a revision of the Fe-Ti two-oxide geothermometer and oxygen-barometer. *American Journal of Science*, 308, 9, 957–1039.
- Ghiorso M.S. & Sack R.O., 1991: Fe-Ti oxide geothermometry: thermodynamic formulation and the estimation of intensive variables in silicic magmas. *Contributions of Mineralogy and Petrology*, 108, 4, 485–510.
- Haggerty S.E., 1991: Oxide textures – A mini-atlas. In: Lindsley D.H. (Ed): Oxide minerals: Petrologic and magnetic significance. *Review in Mineralogy*, 25, 129–137.
- Hammer J.E., 2006: Influence of fO_2 and cooling rate on the kinetics and energetics of Fe-rich basalt crystallization. *Earth and Planetary Science Letters*, 248, 3–4, 618–637.
- Harlov D., Tropper P., Seifert W., Nijland T. & Förster H.J., 2006: Formation of Al-rich titanite (CaTiSiO₄O–CaAlSiO₄OH) reaction rims on ilmenite in metamorphic rocks as a function of fH_2O and fO_2 . *Lithos*, 88, 1–4, 72–84.
- Hurai V., Simon K., Wiechert U., Hoefs J., Konečný P., Huraiová M., Pironon J. & Lipka J., 1998: Immiscible separation of metalliferous Fe/Ti-oxide melts from fractionating alkali basalt: P-T- fO_2 conditions and two-liquid elemental partitioning. *Contributions to Mineralogy and Petrology*, 133, 1–2, 12–29.
- Huraiová M., Dubessy J., Konečný P., Simon K., Král J., Zielinski G., Lipka J. & Hurai V., 2005: Glassy orthopyroxene granodiorites of the Pannonian Basin: tracers of ultrahigh-temperature deep-crustal anatexis triggered by Tertiary basaltic volcanism. *Contributions of Mineralogy and Petrology*, 148, 5, 615–633.
- Klinec A., 1976: Geologická mapa Slovenského rudohoria a Nízkych Tatier (1: 50 000). GÚDŠ, Bratislava.

- Lepage L.D., 2003: ILMAT: an Excel worksheet for ilmenite–magnetite geothermometry and geobarometry. *Computers and Geosciences*, 29, 5, 673–678.
- Lindsley D.H. & Spencer K.J., 1982: Fe–Ti oxide geothermometry: Reducing analyses of coexisting Ti–magnetite (Mt) and ilmenite (Ilm) abstract AGU 1982 Spring Meeting Eos Transactions. *American Geophysical Union*, 63, 18, 471.
- Macdonald R. & Scaillet B., 2006: The central Kenya peralkaline province: Insights into the evolution of peralkaline salic magmas. *Lithos*, 91, 1–4, 59–73.
- Martel C., Pichavant M., Bourdier J.-L., Traineau H., Holtz F. & Scaillet B., 1998: Magma storage conditions and control of eruption regime in silicic volcanoes: experimental evidence from Mt. Pelée. *Earth and Planetary Science Letters*, 156, 1–2, 89–99.
- Mello J. (Ed.), Elečko M., Pristaš J., Reichwalder P., Snopko L., Vass D., Vozárová A., Gaál L., Hanzel V., Hók J., Kováč P., Slavkay M. & Steiner A., 1997: Vysvetlivky ku geologickej mape Slovenského krasu (1:50 000). Vydavateľstvo Dionýza Štúra, Bratislava, 255 p.
- Montel J.M., 1993: A model for monazite/melt equilibrium and application to the generation of granitic magmas. *Chemical Geology*, 110, 1–3, 127–146.
- Nagata T., 1961: Rock magnetism (2nd edition). Maruzen, Tokyo, 350 p.
- Ondrejka M., 2004: Ryolity A-typu silicika v prostredí permsko-triasového kontinentálneho riftingu Západných Karpát: geochemia, mineralógia, petrológia. PhD práca, Manuskript, *Univerzita Komenského Bratislava*, 129 p.
- Ondrejka M., Uher P., Pršek J. & Ozdín D., 2007: Arsenian monazite-(Ce) and xenotime-(Y), REE arsenates and carbonates from the Tisovec-Rejkovo rhyolite, Western Carpathians, Slovakia: Composition and substitutions in the (REE,Y)XO₄ system (X = P, As, Si, Nb, S). *Lithos*, 95, 1–2, 116–129.
- O'Reilly W., 1984: Rock and mineral magnetism. Blackie, Glasgow and London; Chapman & Hall, New York, 220 p.
- Petrík I., Nabelek P.I., Janák M. & Plašienka D., 2003: Conditions of formation and crystallization kinetics of highly oxidized pseudotachylytes from the High Tatras (Slovakia). *Journal of Petrology*, 44, 5, 901–927.
- Powell R. & Powell M., 1977: Geothermometry and oxygen barometry using coexisting iron-titanium oxides: a reappraisal. *Mineralogical Magazine*, 41, 318, 257–263.
- Pupin J.P., 1980: Zircon and granite petrology. *Contributions to Mineralogy and Petrology*, 73, 3, 207–220.
- Putnis A., 1978: The mechanism of exsolution of hematite from iron-bearing rutile. *Physics and Chemistry of Minerals*, 3, 2, 183–197.
- Ryabchikov I.D. & Kogarko L.N., 2006: Magnetite compositions and oxygen fugacities of the Khibina magmatic system. *Lithos*, 91, 1–4, 35–45.
- Rollinson H.R., 1980: Iron-Titanium oxides as an indicator of the role of the fluid phase during the cooling of granites metamorphosed to granulite grade. *Mineralogical Magazine*, 43, 623–631.
- Saito T., Ishikawa N. & Kamata H., 2004: Iron–titanium oxide minerals in block-and-ash-flow deposits: implications for lava dome oxidation processes. *Journal of Volcanology and Geothermal Research*, 138, 3–4, 283–294.
- Samuel M.D., Moussa H.E. & Azer M.K., 2007: A-type volcanics in Central Eastern Sinai, Egypt. *Journal of African Earth Sciences*, 47, 4–5, 203–226.
- Simon A.C., Pettke T., Candelp A., Philip A., Piccoli M. & Heinrich C.A., 2004: Magnetite solubility and iron transport in magmatic-hydrothermal environments. *Geochimica et Cosmochimica Acta*, 68, 23, 4905–4914.
- Smith V.C., Shane P. & Nairn I.A., 2005: Trends in rhyolite geochemistry, mineralogy, and magma storage during the last 50 kyr at Okataina and Taupo volcanic centres, Taupo Volcanic Zone, New Zealand. *Journal of Volcanology nad Geothermal Research*, 148, 3–4, 372–406.
- Shane P., 1998: Correlation of rhyolitic pyroclastic eruptive units for the Taupo volcanic zone by Fe–Ti oxide compositional data. *Bulletin of Volcanology*, 60, 3, 224–238.
- Shane P., Martin S.B., Smith V.C., Beggs K.F., Darragh M.B., Cole J.W. & Nairn I.A., 2007: Multiple rhyolite magmas and basalt injection in the 17.7 ka Rerewhakaaitu eruption episode from Tarawera volcanic complex, New Zealand. *Journal of Volcanology and Geothermal Research*, 164, 1–2, 1–26.
- Spencer K.J. & Lindsley D.H., 1981: A solution model for coexisting iron-titanium oxides. *American Mineralogist*, 66, 11–12, 1189–1201.
- Stormer J.C., 1983: The effects of recalculation on estimates of temperature and oxygen fugacity from analyses of multicomponent iron-titanium oxides. *American Mineralogist*, 68, 5–6, 586–594.
- Sylvester P.J., 1989: Post-collisional alkaline granites. *Journal of Geology*, 97, 3, 261–280.
- Sylvester P.J., 1994: Archean granite plutons. In: Condie K.C. (Ed.): *Archean Crustal Evolution*. Elsevier, Amsterdam, The Netherlands, pp. 261–314.
- Šulgan M., 1986: Praktické použitie Fe–Ti oxidového geotermobarometra (zjednodušený výpočet hodnôt X_{Usp} a X_{Ilm}). *Mineralia Slovaca*, 18, 6, 569–571.
- Uher P., Ondrejka M., Spišiak I., Broska I. & Putiš M., 2002: Lower Triassic potassium-rich rhyolites of the Silicic Unit, Western Carpathians, Slovakia: Geochemistry, mineralogy and genetic aspects. *Geologica Carpathica*, 53, 1, 27–36.
- Vojtko R., 2000: Are there tectonic units derived from the Meliata–Hallstatt trough incorporated into the tectonic structure of the Tisovec Karst? (Muráň karstic plateau, Slovakia). *Slovak Geological Magazine*, 6, 4, 335–346.
- Watson E.B. & Harrison T.M., 1983: Zircon saturation revisited: temperature and composition effects in a variety of crustal magma types. *Earth and Planetary Science Letters*, 64, 2, 295–304.
- Waychunas G.A., 1991: Crystal chemistry of oxides and oxyhydroxides. In: Lindsley D.H. (Ed): *Oxide minerals: Petrologic and magnetic significance. Review in Mineralogy*, 25, 11–68.
- Whalen J.B., Currie K.L. & Chappell B.W., 1987: A type granites: geochemical characteristic, discrimination and petrogenesis. *Contributions to Mineralogy and Petrology*, 95, 4, 407–419.
- Zhu Y., Ogasawara Y. & Ayabe T., 2002: The mineralogy of the Kokchetav 'lamproite': implications for the magma evolution. *Journal of Volcanology and Geothermal Research*, 116, 1–2, 35–61.

Appendix: Reconstitution of primary Ti-rich magnetite composition (example on Fe–Ti oxide polygon 1 in Fig. 5)

The calculated magnetite/ilmenite area ratios in selected grains and a mixing equation were used for reconstruction of the compositional average of the former primary Ti-magnetite. Following procedure was applied to obtain the relevant statistical data:

- A compilation of appropriate iron-titanium oxide textures (trellis-sandwich type) free of inclusions was divided into polygons showing a varying numbers of angles and strictly defined sharp boundaries (Fig. 5A).
- Different greyscale level of digital images converted to B/W binary images (Fig. 5B) from BSE allows the calculation of the ilmenite/magnetite area fractions.
- Calculation of the total square area of each polygon, ilmenite and magnetite square areas and fraction of ilmenite and magnetite square areas using these binary images.

$$X_{\text{Ilm}} = \frac{\text{Area}_{\text{Ilm}}}{\text{Area}_{\text{total}}} \quad X_{\text{Mt}} = \frac{\text{Area}_{\text{Mt}}}{\text{Area}_{\text{total}}} \quad (1)$$

where X_{Ilm} is the fraction of ilmenite square area, X_{Mt} is the fraction of magnetite square area, Area_{Ilm} is the square area of ilmenite, Area_{Mt} is the square area of magnetite and $\text{Area}_{\text{total}}$ is the total square area of polygon.

Figure (5B) shows the selected Fe–Ti oxide texture-polygon [1], which has

a calculated total area of 26 061 pixels, for which the ilmenite (black) makes up 3613 pixels and magnetite (white) makes up 22 448 pixels, thus giving proportional values for ilmenite (X_{ilm}) and magnetite (X_{mt})

$$X_{ilm} = \frac{3613}{26061} = 0.1386 \quad X_{Mt} = \frac{22448}{26061} = 0.8613 \quad (2)$$

(d) Acquired fraction values can be considered to be roughly equivalent to volume fractions which can be converted to weight fraction as follows:

$$m = \rho \cdot P \quad (3)$$

where m is the weight %, ρ is the density ($Mt = 5.2$ and $Ilm = 4.75$ g/cm³) and P is the volume value. The conversion to index number of weight fraction for polygon [1] can be written as follows:

$$m_{ilm} = 4.75 \cdot 0.1386 \quad m_{Mt} = 5.2 \cdot 0.8613 \quad (4)$$

$$\text{Index number} \quad m_{ilm} = \frac{0.658}{5.137} = 0.128 \quad m_{Mt} = \frac{4.479}{5.137} = 0.8719 \quad (5)$$

Therefore the mixing equation takes the form:

$$Oxide_{calc} = (X_{ilm} \cdot Oxide_{ilm}) + [(1 - X_{ilm}) \cdot Oxide_{Mt}] \quad (6)$$

where X_{ilm} is the weight fraction of ilmenite, X_{Mt} is the weight fraction of magnetite, $Oxide_{ilm}$ is the average value of each oxide in ilmenite, $Oxide_{Mt}$ is the average value of each oxide in magnetite, $Oxide_{calc}$ is the calculated concentration of each oxide.

The calculated average composition of primary Ti-rich magnetite (titano-magnetite) in all studied samples shows the magnetite component of 56 mol. % together with ulvöspinel component of 41 mol. % (Tab. 1).